

Article

Adaptation of sequential action benefits from timing variability related to lateral basal ganglia circuitry

Lachlan A. Ferguson,^{1,*} Miriam Matamales,¹ Christopher Nolan,¹ Bernard W. Balleine,¹ and Jesus Bertran-Gonzalez^{1,2,*}

SUMMARY

Streamlined action sequences must remain flexible should stable contingencies in the environment change. By combining analyses of behavioral structure with a circuit-specific manipulation in mice, we report on a relationship between action timing variability and successful adaptation that relates to post-synaptic targets of primary motor cortical (M1) projections to dorsolateral striatum (DLS). In a two-lever instrumental task, mice formed successful action sequences by, first, establishing action scaffolds and, second, smoothly extending action duration to adapt to increased task requirements. Interruption of DLS neurons in M1 projection territories altered this process, evoking higher-rate actions that were more stereotyped in their timing, reducing opportunities for success. Based on evidence from neuronal tracing experiments, we propose that DLS neurons in M1 projection territories supply action timing variability to facilitate adaptation, a function that may involve additional downstream subcortical processing relating to collateralization of descending motor pathways to multiple basal ganglia centers.

INTRODUCTION

For stable environmental contingencies that require more than a single action, animals can learn to perform a series of discrete responses that, as experience accrues, melds the internal boundaries between actions into accurately timed streams of skilled behavior, often expressed as a single unit or “chunk.”^{1–6} In a fluctuating environment, however, behavioral streams must incorporate a sustained degree of variability if they are to remain adaptive.⁷ Animals can show a dramatic variability in the rate of responding that is specifically promoted by the external requirements of the task—such as reinforcement schedule and session duration—rather than by internal motivational states.^{8,9} It has been argued that this variability in performance (or within-organism “noise”) can sustain itself through reinforcement (known as “reinforced variability”), such that fluctuating behavior is instrumental in achieving outcomes.¹⁰ Importantly, behavioral noise is multifaceted in at least two ways: (1) the variation of the number of actions and (2) the variation in the timing of these actions—both of which have been shown to contribute to establishing optimal performance.¹¹ Such forms of behavioral variability therefore constitute a valuable source of change that can support the adaptation of well-established sequential action when environmental conditions demand it.

The modification of well-established action appears to be particularly dependent on motor cortical inputs targeting underlying basal ganglia structures. For example, during the development of overtrained actions, such as habits and skills, the functional priority of cortical projections to distinct basal ganglia regions appears to be reorganized from medial prefrontal cortex and dorsomedial striatum (DMS) to sensorimotor cortices and dorsolateral striatum (DLS).^{12–17} In the context of motor skill learning, corticostriatal afferents targeting the DMS and DLS initially co-engage, but as skills develop, medial associative input strength declines more rapidly and to a greater degree than lateral motor cortical inputs.¹⁸ Beyond the canonical intratelencephalic and pyramidal tract cortical projections reaching the motoric striatum, several recent studies have highlighted the functional importance of subdivisions of these descending projections, including motor corticofugal systems that collateralize over underlying basal ganglia nuclei, such as the DLS, the globus pallidus externa (GPe), and the subthalamic nucleus (STN),^{19–23} opening the door to additional sources of bottom-up motor output processing.

In the striatum, studies recording neuronal activity or assessing function using chemogenetics implicate lateralized striatal regions in the regulation of action chunking and timing.^{24–28} Contributions to the temporal dynamics of well-learned action sequences have also been observed following manipulations of direct pathway projection neuron activity in the DLS (e.g., optogenetic stimulation extends ongoing action sequences),²⁹ whereas chemogenetic inhibition during learning compresses sequences into briefer durations,³⁰ often without impacting the total number of presses within them.²⁷ Similarly, pharmacological DLS inactivation in well-trained animals can preserve action sequence structure while increasing trial-by-trial variability.³¹ Collectively, although evidence strongly supports the contribution of cortical projections

¹Decision Neuroscience Laboratory, School of Psychology, University of New South Wales, Sydney, NSW, Australia

²Lead contact

*Correspondence: lachferguson@gmail.com (L.A.F.), j.bertran@unsw.edu.au (J.B.-G.)
<https://doi.org/10.1016/j.isci.2024.109274>



directly or secondarily targeting DLS neurons in establishing both the structure and timing of well-learned sequences, the way the downstream circuitry promotes further adaptation of action remains unstudied.

Here, we hypothesized that DLS neurons processing motor-related information shape action sequence structure by modulating the construction and temporal variability of action sequences. By implementing a two-lever instrumental paradigm that specifically promotes self-determined variations of sequence length and action timing, we identified that mice construct close-to-optimal sequence lengths with stable inter-press intervals following initial sequence acquisition, then smoothly integrate further behavioral segments into larger action sequences when contingency requirements increase. We found that depletion of a subset of DLS neurons in M1 projection territories destabilized this process by reducing timing variability and overall task success.

RESULTS

As mice build skilled actions, the timing of their sequences adapts with success

The first experiment aimed to characterize the behavioral adaptations that mice make to the timing and efficacy of their performance over instrumental training. To ensure that action timing and performance remained self-paced and uninfluenced by external cues common in instrumental conditioning settings (e.g., pellet delivery sounds), we developed a self-paced chained-sequence task based on the Mechner counting task.^{11,32} Mice were presented with two levers in tandem and earned a reward for a single press on the second 'End' lever, provided they had completed the required number of presses on the first 'Sequence' lever (Figure 1A, top). This allowed the mice to freely decide the duration of their action chains (performed on the Sequence lever) without relying on external cues associated with reward delivery. The requirements on the Sequence lever increased every four sessions from fixed ratio (FR) 1 to FR3 to FR5 across training, whereas the End lever always required one single press (Figure 1A, bottom). General measures of performance in this task, such as lever press rate (Figure 1B) and number of presses per sequence (Figure 1C), significantly increased for the Sequence lever but not for the End lever over the course of training after pretraining (Figure S1A). This was supported by a significant session × lever interaction in both cases (Table S1), demonstrating that mice appropriately biased performance toward the Sequence lever. Mice also significantly increased the rate of rewards earned within each FR schedule (Figure 1D; Table S1), accompanied by a parallel reduction in the number of sequences required to achieve them (Figure 1E), as well as reduced magazine entry rates (Figure S1B; Table S1). These results show that mice clearly distinguished between lever contingencies and adapted well in each phase of the task.

We then assessed if the improved effectiveness in earning rewards coincided with more efficient action sequence timing. To determine what type of changes in timing predominated during the adaptation of action, we measured the peak probability of both individual inter-press intervals (IPIs) within a sequence and whole sequence durations across training (FR3 and FR5). We found that the probability density distribution for IPIs remained stable throughout training, whereas the same function applied to sequence duration shifted to the right as training progressed (Figures 1F, S2A, and S2B). Measures of the action timing peak distribution across training revealed that IPIs remained relatively stable, with only a moderate decline occurring between FR3 and FR5 phases. In contrast, the sequence duration initially declined during early acquisition (FR3), then steadily increased during FR5 training (Figure 1G; Table S1). Given the rise in reward rate, the related decline in the number of sequences, and the elongation of the number of presses per sequence, we expected the likelihood of performing action sequences that ended in reward to increase as training progressed. We calculated the percentage of successful (rewarded) sequences relative to unsuccessful (unrewarded) sequences and found that the former significantly increased within each training phase (FR3 and FR5), reaching 39.11% on average across all training and, after five sessions, plateauing at approximately 50% success on FR5 (Figure 1H; Table S1). Mice were clearly capable of improving the efficacy of their sequences by increasing the chance of performing—at minimum—the required number of presses. It was unclear, however, if the adjustments to the number of actions from unsuccessful to successful trials coincided with adjustments in sequence timing, i.e., whether (1) more presses were added to a fixed period and executed at a faster rate or (2) sequence duration was extended with the addition of lever presses executed at a similar rate. We observed that the latter was the case: when a significantly greater number of presses was implemented for successful sequences (Figures 1I and S1D), the peak sequence duration of successful sequences shifted to significantly longer durations relative to unsuccessful attempts (Figures 1J and S1E; Table S1). These data suggest that when it comes to action timing, over and above changes in inter-press intervals, the modulation of sequence duration seems to be the critical variable when adapting action for success.

Action sequences smoothly allocate performance to meet task requirements

We next examined how successful sequences are constructed when facing a change in schedule. We investigated this by quantifying the frequency of all sequences according to the number of presses per sequence (Figures 2A and 2B). Then, to discern the likelihood of performing a sequence comprised of a given number of presses for either sequence category (i.e., unsuccessful and successful), we independently calculated the probability for each total number of presses per sequence that were performed in either successful or unsuccessful sequences. In probabilistic terms, we found that successful responses were often a two-press segment away from the most frequent unsuccessful sequence, aligning with the prior FR (Figures 2A and 2B, insets). However, regardless of the outcome of the sequences (successful or unsuccessful), frequency distributions of the sequence length showed that the most common unsuccessful sequences were not necessarily two presses shorter than the current contingency. Instead, they fell within a Gaussian-like distribution around the prior contingency. These results indicate that after experiencing increases in contingency, mice demonstrated an ability rapidly to change performance, adapting the distribution of their sequence lengths to meet the new schedule requirements without excessive under- and overshooting.

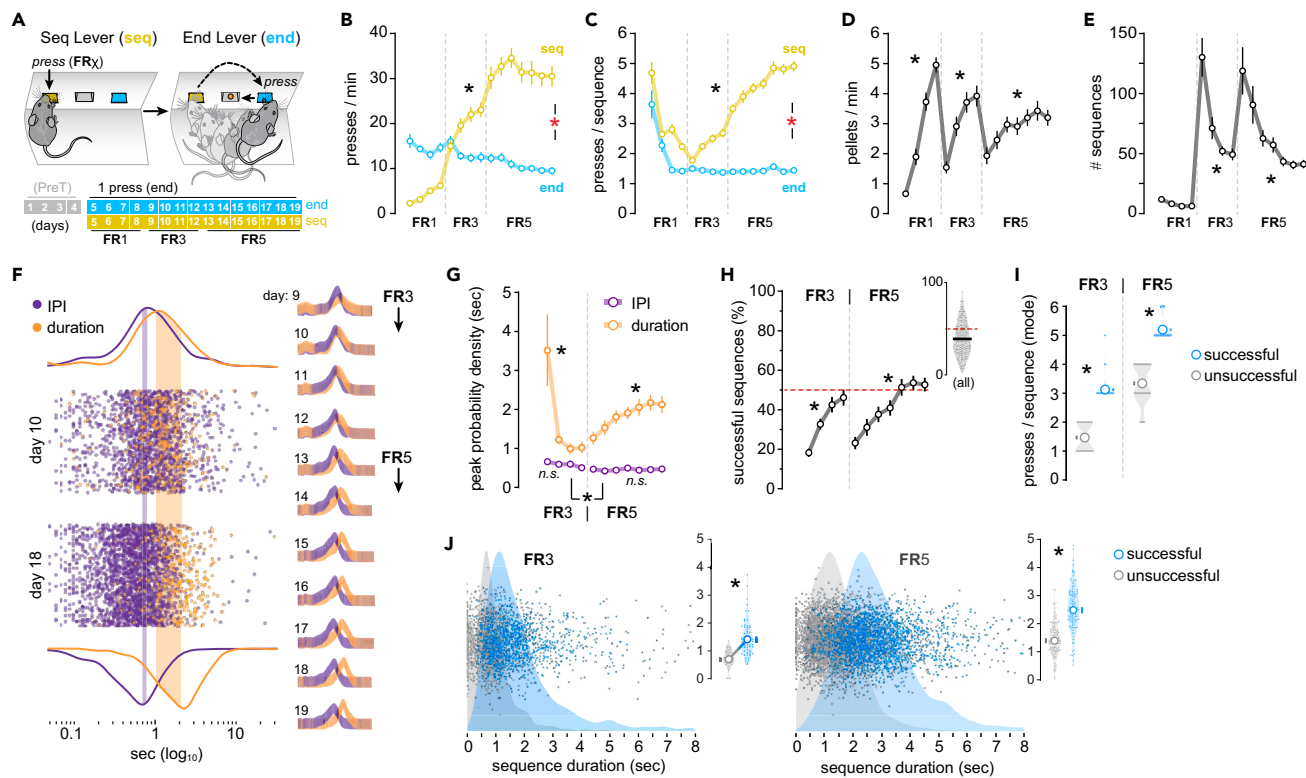


Figure 1. A self-paced sequence task reveals sequence timing adaptations during training

(A) Animals were pre-trained with continuous reinforcement (1 press → 1 reward) on the End lever for four sessions (sessions 1–4, PreT, see Figure S1A). Next, the Sequence lever was introduced on a fixed ratio (FR) 1 schedule for four sessions (sessions 5–8), whereby pressing on the Sequence lever must occur prior to pressing the End lever in order to receive reward. In the following four sessions (sessions 9–12), the press requirements on the Sequence lever increased to FR3. In the final seven sessions (sessions 13–19), the press requirements on the Sequence lever increased to FR5.

(B) Lever press rate measured as presses per minute on each lever type throughout FR1–FR5 training.

(C) Sequence length measured as the number of presses per sequence in both the Sequence and End levers across FR1–FR3 training.

(D) Reward rate measured in pellets per minute. See Figure S1C for the total rewards earned throughout training.

(E) Total number of sequences performed throughout FR1–FR5 training.

(F) Scatterplot of every IPI and sequence duration value (to \log_{10}) on the Sequence lever for all animals in an example FR3 (day 10) and FR5 (day 18) session, with probability density function curves that follow the distribution of sequence durations, indicating peak differences (shaded). Right diagrams show the probability density function curves on each day of FR3–FR5 training. See Figures S2A and S2B for individual days.

(G) IPI and duration peaks of probability density (PPD) across FR3 and FR5 training averaged across individual subjects.

(H) Percentage of sequences that successfully resulted in reward in FR3 and FR5 sessions across training and in all FR3 and FR5 training sessions collapsed (inset). Red dashed line denotes 50%.

(I) Most frequently occurring (modal) number of presses in either unsuccessful or successful sequences for both FR3 or FR5 training. Truncated violin plots are fitted to data points (shaded).

(J) Scatterplot with probability density function curves (shaded) of sequence duration for every unsuccessful (unrewarded) and successful (rewarded) sequence performed by the entire cohort during FR3 (left) and FR5 (right). Insets show PPD for each animal and day during FR3 (left) and FR5 (right) training. Data are mean ± S.E.M. *Significant overall/simple effect (black) and interaction (red). N.S., not significant (Table S1).

Next, we explored the way lever press responses were chunked during action sequence learning and whether temporal gaps between sequence segments emerged as animals adapted their actions to new ratio requirements.³ For this, the duration of each segment within successful sequences was arranged chronologically (following the order in which each sequence occurred within a session). To observe the relationship between the chronological progression of successful sequences and the duration of their constituent segments, we analyzed their linear relationship over both FR3 and FR5 training (Figures 2C, 2D, and S3). We found that during FR3 training—when sequences are first acquired—the duration of the first FR1-3 segment (time between presses 1–3) significantly declined over training (Figures 2C and S3A; Table S1). In contrast, during FR5 training—when FR3 requirements were already frequently met and two extra presses were required for reward—the duration of the FR3-5 segment (time between presses 3–5) was the same as the FR1-3 segment in late FR3 training (~1 s; Figure 2D) and remained constant throughout the rest of training (Figures 2D and S3B; Table S1). In light of the observed disparities in the evolution of FR1-3 and FR3-5 segments of successful sequences, we investigated if the two segments were implemented as discrete units with a pause between them or if they were smoothly integrated into an extended single sequence of action. We found that the time in-between the two segments

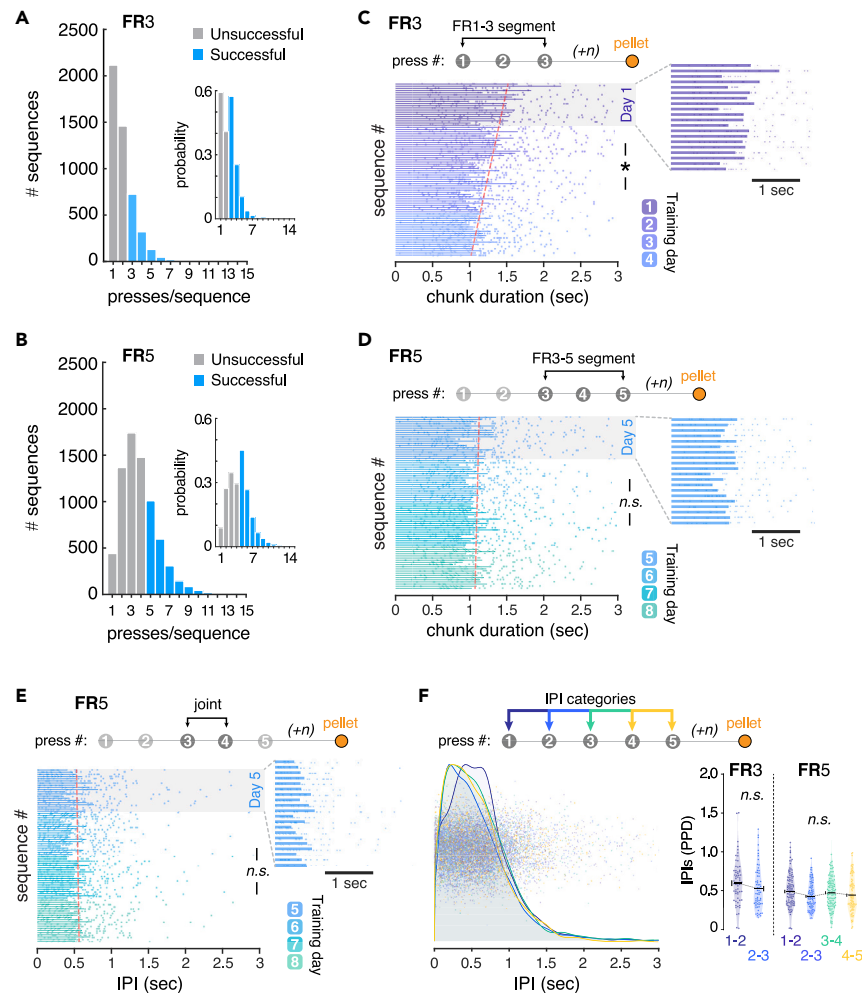


Figure 2. Successful action dynamics adapt as task requirements increase

(A and B) Frequency histograms showing the total number of sequences performed on the sequence lever according to the number of presses per sequence during FR3 (A) and FR5 (B) training. Insets show the probability distribution of the same successful and unsuccessful sequence categories during FR3 (A, right) and FR5 (B, right) training quantified independently to illustrate within-category probabilities.

(C–E) Duration of successful subsequence intervals ranging from presses 1–3 (FR1-3 segment, C), presses 3–5 (FR3-5 segment, D), and presses 3–4 (joint, E) arranged chronologically across the first four sessions of FR3 and FR5. Data are the duration of each sequence by each mouse (dots) and the average across mice (bars). A linear regression model highlighting the chronological trend is fitted to the data (red dashed line). Insets are an enlarged view of the first session of the corresponding fixed ratio schedule.

(F) Scatterplot with probability density function curves (shaded) of IPIs between 1-2, 2-3, 3-4, and 4-5 press transitions for every successful sequence performed by the entire mouse cohort during FR3 and FR5 training (left). Peak probability density (PPD) of relevant IPIs in successful sequences for each training session (dots) plotted for both FR3 and FR5 (right). n = any number of presses before reward. *Significant overall/simple effect (black) and interaction (red). N.S., not significant (Table S1).

(i.e., the “joint” IPI; between presses 3 and 4) remained invariable as rewarded experience accrued across FR5 training (Figures 2E and S3C; Table S1). Furthermore, we found that the different IPI categories across successful sequences were mostly indistinguishable from each other, including the joint IPIs connecting FR1-3 and FR3-5 segments (Figure 2F; Table S1). Collectively, these data reveal that mice smoothly integrated new sub-sequence segments with previously acquired sequence prototypes to immediately form extended sequences, all without the assistance of reward delivery cues.

Interruption of DLS neurons in M1 projection territories speeds up sequential action

Functional assays, such as lesion and chemogenetic suppression, indicate that the DLS governs a variety of roles relevant to optimizing task performance in sequence-based instrumental conditioning, ranging from skilled action kinematics, speed and variation of action sequences, habit learning, and the accurate acquisition of a serial order.^{16,27,31,33–35} Similarly, the M1 and its connectivity with the DLS has also been

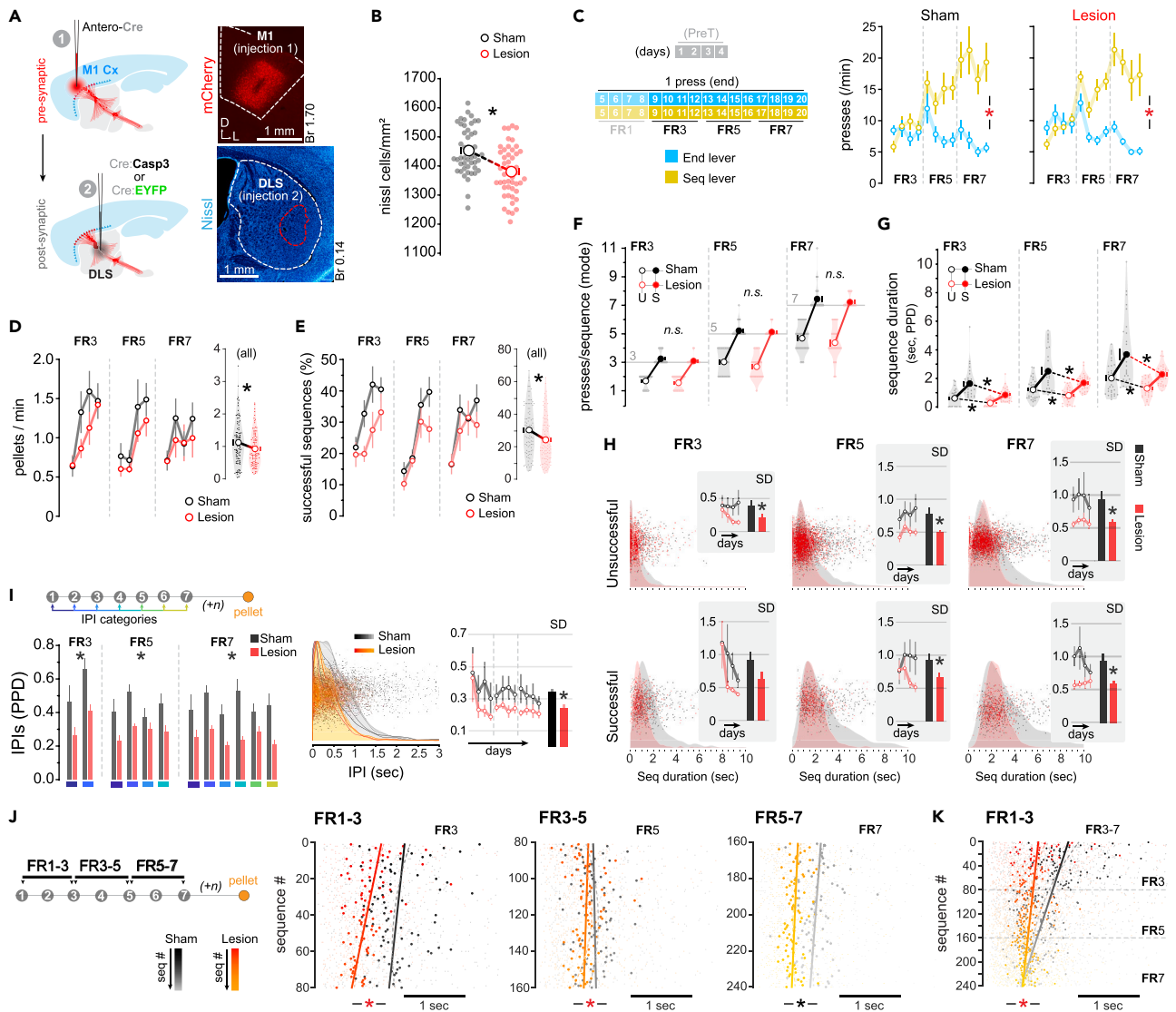


Figure 3. Specific interruption of the M1 → DLS circuit alters the temporal dynamics of action sequences

(A) Schematic of the M1 → DLS circuit lesion strategy. (1) An anterograde AAV expressing Cre (Antero-Cre) was injected into the M1. (2) An AAV expressing either Cre-dependent synthetic procaspase taCasp3 (Cre:Cas3; Lesion group) or Cre-dependent EYFP (Cre:EYFP; Sham group) was then injected into the DLS. Top-right: confocal micrograph showing expression of Antero-Cre virus in the M1 injection site revealed by mCherry. Bottom-right: confocal micrograph showing the usual extent of the lesion at the Cre:Cas3 injection site in the DLS revealed by Nissl labeling.

(B) Nissl-based cell density quantification within DLS injection site.

(C) Left: animals began pre-training with continuous reinforcement (CRF) on the End lever (L_{end}) for four sessions (PreT), then shifted to the tandem task on the Sequence lever (L_{seq}) progressing through FR1 → FR3 → FR5 → FR7 schedules every four sessions. Right: lever press rate measured as presses per minute on each lever type throughout FR3 → FR7 training in each group. For sessions 1–4 (PreT), see Figure S4C.

(D) Reward rate (press/min) throughout FR3 → FR7 training. Inset shows data from the three schedules collapsed.

(E) Percentage of successful sequences across FR3 → FR7 training. Inset shows data from the three schedules collapsed.

(F) Most frequent (modal) number of presses in a sequence (press/sequence) for both Successful and Unsuccessful sequences in FR3, FR5, and FR7 schedules.

(G) Sequence duration (peak probability distribution, PPD) for both Successful and Unsuccessful sequences in FR3, FR5, and FR7 schedules.

(H) Scatterplot with PPD curves (shaded) of sequence duration for every unsuccessful (top) and successful (bottom) sequence produced by the entire cohort during FR3, FR5, and FR7 phases. Insets show standard deviation (SD) across training sessions and a summary bar graph of all sessions within the indicated schedule.

(I) Left: schematic for quantification of IPIs within a sequence. Data (bottom) show the PPD of the relevant IPIs for successful sequences in each schedule. Center: scatterplot with PPD functions (shaded) of IPIs between the indicated press transitions for every successful sequence performed by the entire cohort as FR3 → FR7 training progresses (color coded). Right: standard deviation (SD) across FR3 → FR7 training. Inset shows a summary bar graph of all sessions collapsed.

Figure 3. Continued

(J) Duration of successful subsequence intervals ranging from presses 1–3 (FR1-3 segment, left), presses 3–5 (FR3-5 segment, center), and presses 5–7 (FR5-7 segment, right) arranged chronologically across FR3, FR5, and FR7 sessions. Data are the duration of each sequence by each mouse (small dots) and the average across mice (larger dots). A linear regression model highlighting the chronological trend is fitted to the data (line). The change in color in each group's dataset reflects throughout training such that the color gets lighter as sessions progress (see legend to the bottom-left).

(K) Duration of the first successful subsequence segment (FR1-3 segment) throughout the entire FR3→FR7 training. n = any number of presses before reward. Data are mean \pm S.E.M. *Significant overall/simple effect (black) and interaction (red). N.S., not significant (Table S1).

implicated in the acquisition and governance of the constituent components of skilled action sequences.^{18,21,36} We investigated whether post-synaptic targets of M1 projections to the striatum contributed to modulating action time during sequence learning and whether this influenced task success. In adult mice, we selectively lesioned DLS neurons receiving M1 input through an AAV-based circuit-specific lesion approach, which combined anterograde transport of Cre with Cre-dependent lesion^{37,38} (Figure 3A). A first adeno-associated virus (AAV) expressing anterograde traveling, *trans*-synaptic WGA-Cre (AAV2-EF1a-mCherry-IRES-WGA-Cre; Antero-Cre) was injected into the M1 (Figure S4A), followed by delivery of a second AAV into the DLS, which expressed either Cre-dependent procaspase 3 (AAVFlex-taCasp3-TEVp; Cre:Casp3) or Cre-dependent EYFP (AAV5-EF1A-DIO-eYFP; Cre:EYFP) (Figure S4B). Cre-Casp3-injected mice (Lesion group) showed a significant reduction of neuronal density in a defined area of the DLS compared with Cre:EYFP mice (Sham group) (Figure 3B). When exposing these animals to the self-paced sequence task, we found that mice from both the Lesion and Sham groups appropriately biased lever press performance toward the Sequence lever as sequence training progressed from FR3 to FR7 (Figure 3C), revealed by a strong session \times lever interaction in both groups (Table S1). On the other hand, a summary of task success across all sequence training (FR3–FR7) showed that M1-driven DLS-lesioned mice earned rewards at a slower rate (Figure 3D; Table S1) and performed sequences with a lower percentage of success relative to Sham controls (Figure 3E; Table S1), without impacting the total number of earned rewards or magazine entries per session (Figures S4D and S4E). Despite this reduced percentage of successful actions, the Lesion group showed no modal differences in the number of presses per sequence relative to the Sham group when performing either unsuccessful or successful sequences (Figure 3F; Table S1). At the population level, the distribution of the number of presses per sequence showed that rewarded sequences most frequently matched the FR schedule for both groups, indicating that they do not greatly “overshoot” the FR thresholds (Figures S4J–S4L). Moreover, as would be predicted by the reduced % of successful sequences (Figure 3E), the DLS lesion group performed more sequences below the FR threshold than Sham controls. By contrast, the overall timing of these sequences was altered, such that both unsuccessful and successful sequences were faster in lesioned mice (Figure 3G; Table S1).

DLS neurons located in M1 projection territories support action timing variability

Next, we explored the relationship between sequence speed increases and the variability of their execution as a source of explanation for the reduced success of M1-driven DLS lesioned animals. We found that the Lesion group maintained more consistent durations across unsuccessful and successful sequences compared with Sham controls throughout training (Figure 3H), the latter group showing significantly more variable sequence durations of either type at each phase of training (Table S1). Consistent with a variability-based explanation of task success, within-subjects analysis showed that successful sequences were significantly more variable than unsuccessful sequences in both groups (Figure S4F; Table S1). Further linear regression analysis showed that although successful sequence duration variability declined as task success increased for both groups, the slope of such decline was significantly less pronounced in M1-driven DLS-lesioned mice (Figure S4G; Table S1).

We then sought to clarify if, in successful sequences, the limited timing repertoires promoted by M1-driven DLS lesions generalized to whole sequence spans or if action timing limits were present in specific behavioral units within the sequence. By sorting IPIs according to position in the sequence and comparing their differences within each training schedule, we found a general significant decrease in IPI time following DLS lesions across training, with no differences between the IPIs according to position in the sequence for either FR5 or FR7 training (Figure 3I; Table S1). Moreover, similar to the reductions in variability identified in whole sequences, a significant reduction in the variability of the IPIs in successful sequences was observed following lesion (Figure 3I, right panel; Table S1). Further sequence structure analysis showed a reduced duration for the FR1–3 segment (press 1–3) during FR3, for segment 2 (press 3–5) during FR5, and for segment 3 (press 5–7) during FR7 in the DLS lesion group, which significantly diverged from the Sham group as the task progressed through FR3 and FR5 (Figure 3J). Importantly, our analysis of the evolution of the FR1-3 segment—which we observed undergoes temporal change during initial action sequence acquisition in our previous experiment—revealed a highly suppressed rate of change in DLS-lesioned mice, such that early training action speeds more closely resembled later training speeds relative to the significantly increasing speeds found in Sham controls (Figure 3K; Table S1). Notably, this effect was not observed during the later acquisition of segment 2 (press 3–5) or the duration of a successful sequence as a whole (Figures S4H and S4I). Overall, our results showed that M1-driven DLS disruption interfered with the successful construction and adaptation of action sequences in response to an increasing lever press requirement by reducing the optimal range of action speed and variation.

Motor cortical projections form multi-stage connections with the basal ganglia

An important consideration for disentangling corticostriatal function in adapting action sequence dynamics during learning is the likely involvement of subcortical bottom-up processing, something that, based on recent literature, could be promoted by collateralized

connectivity in motor cortical descending pathways. For example, pyramidal tract neurons originating from layer V in the motor cortex are known to strongly collateralize to the subthalamic nucleus (STN), forming a “shortcut” into the basal ganglia commonly known as the hyper-direct pathway.^{39,40} Additionally, corticofugal projections are also known to emit accessory collaterals to more upstream basal ganglia structures such as the GPe or the striatum itself.^{19,21,22} These collateral links to downstream basal ganglia nodes are thought to supply efference copies of ongoing pyramidal tract motor commands, a process that can be key to adjusting the temporal limits of sequential action.^{21,40} We sought to clarify whether motor cortical projections—such as those targeting the DLS pointed out in our study—were also represented in downstream collateral networks of descending corticofugal pathways. We first revised the relative densities of motor cortical axons arborising through diverse basal ganglia structures using the Allen Mouse Brain Connectivity Atlas,⁴¹ which combines eGFP anterograde viral tracing with serial two-photon tomography throughout the entire brain. We selected three different cortical injection assays (spanning the M1, M2, and dorsal agranular insular area [AId] regions) based on their preference of projection to the STN (Figures 4A–4C). EGFP-labeled axons in all three assays densely innervated several subcortical structures, particularly the DLS and lateral areas of the globus pallidus externa (lateral GPe) (Figure 4B). Quantification of EGFP fluorescence identified that, across subcortical structures, the STN, striatum, and GPe consistently had the three highest projection densities over the three assays (Figure 4C).

We then investigated whether these regions (STN, striatum, and GPe) were simply parallel cortical targets or in fact shared collaterals of the same corticofugal neurons. For this, we implemented a quantitative connectivity approach based on the retrograde transport of a Cre-expressing virus (AAV-hSyn-HI-eGFP-Cre-WPRE-SV40) injected at the most downstream target (STN, Figures S5A and S5B), followed by anterograde transport of a Cre-dependent reporter virus (AAV-hSyn1-FLEX-mGFP-2A-synaptophysin-mRuby) injected at the origin of the corticofugal pathway (M1) (Figure 4D). Because the virus causes Cre-dependent anterograde expression of mRuby in synaptic terminals,^{43,44} this method allowed us to quantify the distribution of any mRuby-labeled synaptic boutons in projections collateral to and within the mainstream projection targeting of the STN. Consistent with our previous analysis, we detected dense mRuby puncta in both DLS and lateral GPe, in addition to the final target STN (Figure 4E). Our particle density analysis (Figure 4F) showed that the total number of mRuby+ synaptic boutons was greater in the collateral projections to the striatum and GPe compared with the STN, with the greatest number occurring in the striatum (Figure 4G, purple trace) (Table S1). In contrast, the relative density of synaptic boutons within their regional space was greatest in the STN compared with the striatum and GPe (Figure 4G, red trace) (Table S1). The reconstruction of the distribution of mRuby+ terminals into particle density maps showed that the greatest synaptic densities occurred within the lateral segments of the striatum and GPe, whereas synaptic territories remained central in the final target STN (Figures 4H and S6). We sought to confirm the existence of descending motor neurons emitting multi-stage collaterals into the basal ganglia by using the MouseLight Neuron Browser resource⁴² (Janelia Farm, HHMI). We searched for neurons residing in M2/M1 cortical areas that emitted parallel projections to the dorsal striatum, GPe, and STN (with >10 axonal endpoints in each, indicating a significant connectivity) (Table S3, search #1). Out of the 1,227 neurons in the database, our search identified one prototype neuron that satisfied these criteria, suggesting that a population of motor cortical neurons can indeed reach out to all three basal ganglia structures simultaneously in their path to the brainstem (Figure 4I). Searches considering only one collateral to either the dorsal striatum or the GPe provided only a single additional neuron in each case, suggesting that cortical populations targeting either one or both structures before reaching the STN could have equivalent densities (Table S3, Search #1, #1a, and #1b). 3D reconstruction of the multi-stage projecting neuron confirmed the presence of axonal endings in DLS, GPe, and STN (Figure 4J) and also allowed identifying additional targets in the parafascicular nucleus of the thalamus as well as the upper brainstem (Figure 4K).

In light of the presence of off-target labeled neurons in thalamic areas surrounding the STN in our first experiment (see Figures S5A and S5B) and the possible confounds introduced by the dense corticothalamic circuitry, we sought to ensure the specificity of our findings by conducting additional searches in the MouseLight Neuron Browser that terminated in the various thalamic regions surrounding the STN (Table S3 Searches #2–16). Nearly all of the additional searches provided no result, including searches terminating in VMN, VPC, VPL, VPM, and ZI, emphasizing the weight and significance of M2/1 → STN neurons collateralizing onto various basal ganglia stations (Figures S5C and S5D). The only exceptions were two neurons identified in search #7 (Source: M1cx and M2cx; Targets: DStr and VMN), which represent the confluence between two major projection systems in the brain (corticostriatal and corticothalamic).

Collectively, our data extend recent reports showing upstream cortico-basal ganglia connectivity^{19,21,22,42} and reveal that the cortical descending pathway originating in motor regions can indeed send shared projections to multiple basal ganglia stations. These results support the growing literature emphasizing accessory collateral networks of motor corticofugal systems as important players for the modulation of action timing.

DISCUSSION

Maturation of action sequence timing

A useful behavioral strategy for efficiently exploiting long-standing environmental contingencies often involves enacting accurately learned streams of action executed swiftly. In our study, we found that the within-sequence rate of rewarded actions clearly improved with training, although this was predominantly restricted to the IPI speed of the FR1-3 segment. Any new addition to this “scaffold” remained invariant, including the “joint” (IPI between segments) that melds the first sequences performed in FR3 schedules with longer sequences in FR5 schedules. As lever press requirements increased, mice added segments to successful responses by shifting the distribution of their sequence length away from previously successful sequence lengths and toward currently successful sequence lengths, enabling them to more frequently meet the new FR schedule requirements. This high degree of internal cohesion,³² both within and between the units of action in a sequence, suggests that the integration of segments into whole sequences occurs smoothly, without disruption to the consistent timing

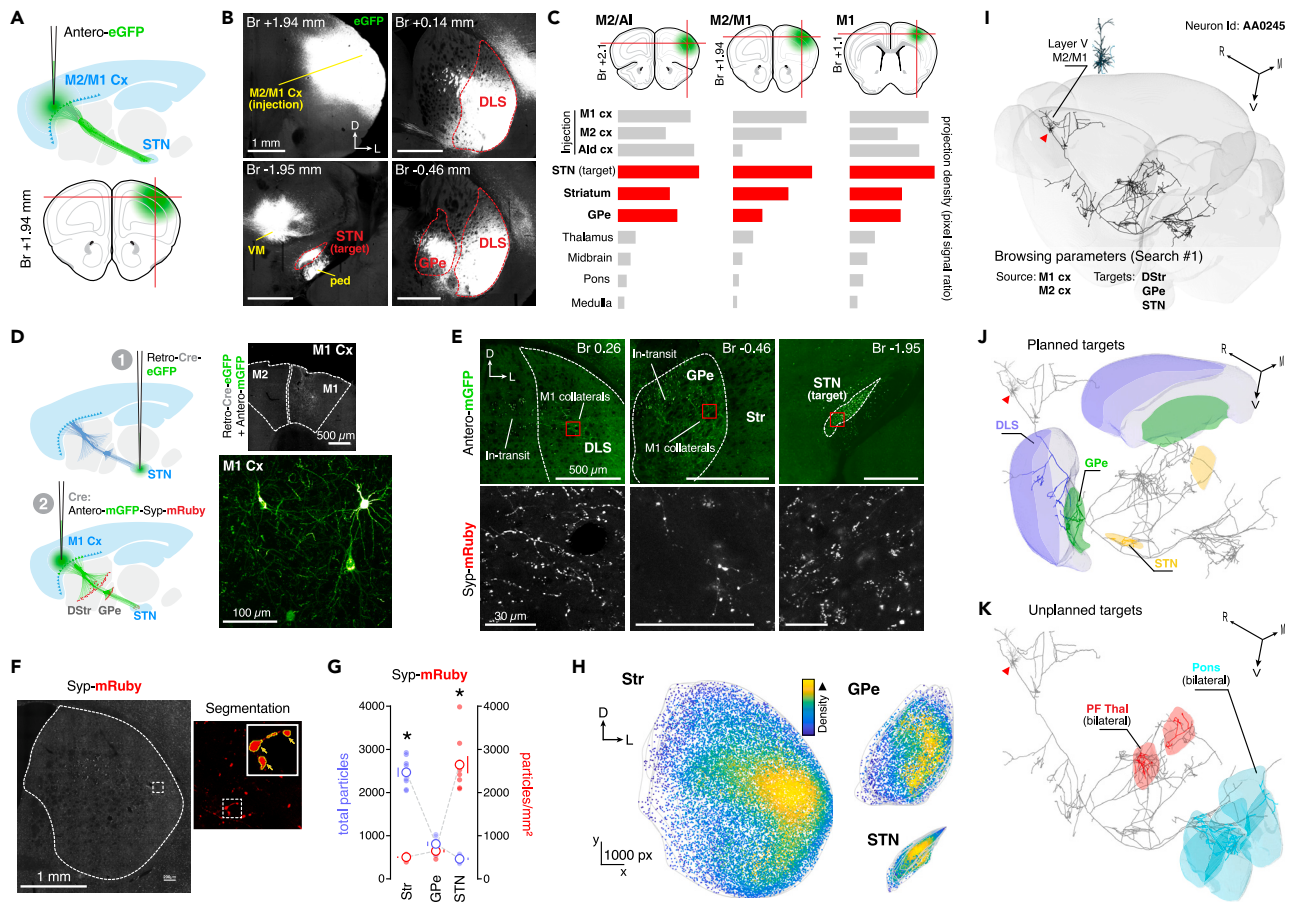


Figure 4. Motor corticofugal projections send shared collaterals to the DLS, GPe, and STN

(A–C) Anterograde tracing study using the Allen Mouse Brain Connectivity Atlas database.⁴¹ Three different cortical injection assays targeting the STN were identified (Source: M1 and M2; Target: STN; see STAR methods). (A) Experimental diagram on one of the assays showing the injection site onto M2/M1 cortex and expected transport of an anterograde reporter virus reaching the STN (antero-eGFP).

(B) Example two-photon tomography images of eGFP expression in the M2/M1 injection site (top-left), the DLS (top-right), the STN (bottom-left), and the GPe (bottom-right) (experiment number 180709942).

(C) Schematic for M2/agranular insular cortex (AI) (top-left), M2/M1 (top-center), and M1 (top-right) injection sites with corresponding projection density quantifications throughout various brain areas. Data are extracted from experiments 180719293 (left), 180709942 (center), and 100141780 (right). Projection densities for cortical regions around the injection site (“Injection”) are listed first, followed by the three highest density regions (red)—including the site of target search (STN)—followed by other representative high-density regions.

(D) Schematic depicting the viral tracing strategy used to identify accessory targets in corticofugal pathways: (1) a retrograde AAV expressing Cre-eGFP was injected in the STN. (2) An anterograde AAV expressing Cre-dependent mGFP and synaptophysin (Syp)-mRuby (labeling presynaptic boutons) was injected in the M1. Right panels are confocal images showing GFP expression in the M1. See Figure S5 for quantification of STN targeting.

(E) Spinning disk confocal images of anterograde-mGFP in the striatum (top-left), GPe (top-center), and STN (top-right); Syp-mRuby-labeled terminals in each region (bottom panels).

(F) Spinning disk confocal image showing Syp-mRuby clusters segmented for particle analysis (see STAR methods).

(G) Total particles and particle density (particles/mm²) quantification for DStr, GPe, and STN regions. Mean ± S.E.M. *p < 0.05.

(H) Particle density maps overlaid for each region (3x slice/animal; n = 3) on side ipsilateral to STN and M1 injection sites. See Figure S6 for individual maps.

(I–K) Identification of a motor corticofugal neuron targeting multiple basal ganglia structures on its path to the brainstem in the MouseLight Neuron Browser.⁴² (I) 3D reconstruction of the full axonal arborization of the identified Layer V cortical neuron (Id: AA0245, <https://doi.org/10.25378/janelia.5527657>), the soma of which is located at the interface between M2 and M1 cortices. This neuron was identified by browsing M2/M1 cortex as the source and dorsal striatum + GPe + STN as targets (>10 axonal endpoints in each; see Table S3). (J) AA0245 neuron’s axonal path with superimposed DLS, GPe, and STN (planned targets). Axonal end segments contained within each region are colored-matched. (K) AA0245 neuron’s axonal path with superimposed parafascicular thalamus (PF Thal) and Pons (unplanned regions in original search). Axonal end segments contained within each region are colored-matched. Red arrowhead points at the soma (M2/M1 region). Axes point to rostral (R), medial (M), and ventral (V) areas.

of consecutive actions, possibly signaling the onset of more automatized action that occurs in moderate to well-trained animals.⁴⁵ Given the consistency of action timing after the initial fixed ratio schedules and the absence of reward cues or time penalties in this task, skilled action timing—based strictly on learned internal estimates of fixed ratios—appears to be transferred when updating contingencies.

DLS neurons in M1 projection territories may tune action rate and variance

Considering the anatomical evidence and arguments supporting meaningful functional interactions between the motor cortical regions and diverse basal ganglia centers, and the effects on action timing we observed following M1-driven DLS lesion, we suggest that DLS processing of motor cortical information may function to stabilize/destabilize the temporal boundaries of learned sequence durations by allocating the minimum level of variability required for explorative performance. The primary evidence for this view comes from the behavioral effects induced by specific ablation of the DLS neurons in territories receiving M1 projections. We found that this selective ablation did not alter the number of actions within successful or unsuccessful sequences *per se*, instead it induced proportionally faster sequences with less varied durations that ultimately made mice less effective at earning reward (i.e., a slower reward rate and a greater proportion of unsuccessful actions). Perhaps unsurprisingly, we found that, in the development of skilled actions, the timing of successful action sequences was more reliable (i.e., less variable) as task performance improved. However, when comparing the variability of unsuccessful actions relative to successful performance within-subjects, we show that both Sham and DLS lesion groups increased the variability of successful sequence durations, indicating that increased variation is a component of successful performance. Consistent with this argument is the observation that, in the less successful DLS lesion group, there was an overall reduced variance. The relationship between action timing variability and task success, therefore, may not be as simple as expecting variance to decline as task accuracy improves; rather, a broader baseline level of variance in action timing-space may be leveraged to expand the repertoire of available actions in action selection-space.

One key example from the literature that implicates timing mechanisms in action performance is outlined in Scalar Expectancy Theory (SET), with its pacemaker-accumulator model denoting a role of an internal clock mechanism used for regulating the pacing and regularity of actions.^{46,47} The theory posits a pacemaker generating pulses at consistent intervals are accumulated, then used to gauge time intervals, subtly influencing the rhythm and sequence of actions.⁴⁸ Rather than action “counting,” a DLS lesion could conceivably impair time “counting” of accumulated intervals of lever pressing, overall reducing task success. Here, sub-optimal estimates of time spent performing the action sequence or a reduction in the capacity to vary timing enough to exceed previously reinforced durations (particularly when moving up FR schedules) could result in sub-FR threshold performance. SET’s emphasis on memory and decision processes, where past timing experiences are stored and influence future action timings, suggests that even in non-timing-centric tasks, the internal representation of time can play a critical role.

The waning yet ongoing M1 → DLS input observed in other studies of motor skill behavior¹⁸ suggests that this circuitry continues to modulate action sequence learning, potentially via its contribution to the degree of encoded variability¹⁰ and its capacity to extend action sequence duration. Functional evidence for the role of the canonical cortico-subthalamic hyperdirect pathway in mice shows that motor cortical targets to the STN exert general inhibitory control over action; for example, lesions induce hyperlocomotor activity, and optogenetic activation leads animals to stop prematurely in a locomotion task.^{49,50} Similarly, some prior evidence suggests that subcortical processing (such as the STN target of the hyperdirect pathway) plays a similar role in the optimization of behavior by tuning action suppression. One proposed explanation for these inhibitory effects comes from the “hold your horses” model, which confers the STN with the capacity to “buy time” when deliberating over difficult choices, improving task accuracy.^{51–54} Although ascribing a general inhibitory function to this pathway could help explain the elevated rate of sequential action and reduction in task success rate following M1-driven DLS lesion, it does not capture the reduced variability effects we observed. More generally, subcortical circuitry is well placed not only to provide the extra action time that is required for sequences to incorporate additional presses and enhance the likelihood of their success but also to modulate the variability of action timing, perhaps directly through interactions with the M1 → DLS network or through broader basal ganglia-thalamo-cortical processing. Here, a greater range of possible action sequence durations might be expected to facilitate successful acquisition of the target sequence. To further investigate the role of action suppression and timing variability, future studies of this kind should consider microstructural movement velocities during the sequence of presses.

Anatomy of corticofugal accessory collaterals

To expand on the anatomical understanding of the dorsolateral striatal environment and its relationship with other known contributors of action timing, this study provided evidence of a direct interaction between lateral corticostriatal circuitry and the downstream basal ganglia network. By implementing a dual-viral tracing approach in which M1 cortical neurons projecting to the STN were first labeled in isolation and then their synaptic terminals subsequently mapped, we were able to observe the preferential ramification of the lateral territories of the striatum and GPe by long-range pyramidal tract collaterals. This method identified collaterals to both the DLS and the GPe, with highest synaptic volumes in the DLS, extending previous research.^{19,21,22,42} Although our method could not distinguish M1 → STN projections with independent collaterals to DLS or GPe from collective M1 → STN projections with collaterals to both, a search in the MouseLight Neuron Browser database⁴² identified one neuron located at the M2/M1 interface that emitted collateral axonal terminals to the DLS, GPe, and STN, suggesting that such multi-stage corticofugal neurons exist and may be relevant for basal ganglia processing. Additional searches limited to only one collateralization before reaching the STN (i.e., either dorsal striatum or GPe) revealed only one more neuron in each case, suggesting that corticofugal neurons reaching out to all three areas constitute a relatively common population of corticofugal systems collateralizing to the basal ganglia. Of note, we found that this same neuron also provided substantial innervation to the parafascicular thalamic nucleus

(PF), an integrant of the midline thalamic nuclei that is particularly well connected with the dorsal striatum.^{55,56} Control searches of neurons collateralizing to the basal ganglia but reaching various thalamic regions instead of the STN produced no results, emphasizing the importance of multi-stage collateralization of corticofugal projections specifically involving the STN. All in all, the anatomical finding of shared connectivity suggests that the DLS and GPe may be responsible for processing some of the action timing information that has typically been attributed to exclusive collaterals to the STN—the so-called hyperdirect pathway. It is possible, however, that the local integration of this timing information in downstream structures may differ. For example, the local inter-cellular interactions between D2-SPNs and D1-SPNs within the striatum⁵⁷ and between prototypic and arky pallidal cells within the GPe⁵⁸ have been implicated in adaptive learning and locomotion functions, respectively. The importance of these “upstream” targets of the accessory corticofugal projections aligns with similar descriptions of basal ganglia function described in the *center-surround model*,⁴⁰ in which information is processed in a feedback loop that differentially recruits direct, indirect, or hyperdirect pathways traversing “forward” and “backward” through the basal ganglia to control motor performance. Similarly, in rats, *race models* of basal-ganglia-driven behavioral response inhibition describe competition between Go, Stop, and Pause signals emerging from striatum, GPe, and STN, respectively, from which the timing of each competing signal is integral to the eventual behavioral output.^{59–61} Presently, using models of the basal ganglia to predict the impact of multiple corticofugal collateral inputs within the circuitry is speculative and requires further experimentation. For example, simultaneous *in vivo* recordings could demonstrate the temporal relationships of downstream firing that occur in response to excitation from a motor cortical input ubiquitous to DLS, GPe, and STN regions—further informing interpretations of *race models*. Just how the supply of shared motor cortical information to multiple basal ganglia nuclei governs function, both locally and at the circuit level, remains to be understood. Nevertheless, such broad projections suggest a widespread and coordinated integration of motor cortical efference copies, a process that is likely essential for adapting on-going streams of behavior throughout learning. Overall, the anatomical mapping of shared striatofugal collaterals to various basal ganglia structures in conjunction with action timing effects observed following M1-driven DLS lesion provides an interesting new avenue for future experiments that connect the functional contribution of corticofugal-basal ganglia networks to action timing and its role in behavioral sequences of action.

Limitations of the study

Variability of action selection can be encoded as an operant function,⁶² and reinforcement of variations in lever press sequences have been shown to help rats learn more complex target sequences,¹⁰ suggesting that variability in performance can improve the acquisition of complex behavioral patterns. Although the present study identified a suppression of timing variability and task success in the DLS lesion groups, timing variability was not a task-relevant dimension directly—in that it was not instrumental in successfully attaining reward. Although the direction of causality cannot be determined from this particular paradigm, it contributes to a literature that implicates timing-variability-based mechanisms in the success/failure of action performance. Moreover, in addition to analyzing the time between presses as a measure of sequence speed (found in this study), measures of forelimb movement speed during and between pressing could illuminate a nuanced distinction between “buying time” between actions and the inherent velocity of actions, both phenomena being capable of varying IPI and sequence durations. Future research could benefit from microstructural analysis using animal pose estimation software paired with video surveillance of action performance.

STAR★METHODS

Detailed methods are provided in the online version of this paper and include the following:

- KEY RESOURCES TABLE
- RESOURCE AVAILABILITY
 - Lead contact
 - Materials availability
 - Data and code availability
- EXPERIMENTAL MODEL AND STUDY PARTICIPANT DETAILS
- METHOD DETAILS
 - Behavioral procedures and analysis
 - Viral procedures
 - Tissue processing and immunofluorescence labeling
 - Image acquisition and quantitative analysis
 - Allen Mouse Brain Connectivity Atlas resource methodology
 - MouseLight Neuron Browser resource methodology
- QUANTIFICATION AND STATISTICAL ANALYSIS

SUPPLEMENTAL INFORMATION

Supplemental information can be found online at <https://doi.org/10.1016/j.isci.2024.109274>.

ACKNOWLEDGMENTS

We thank Jennifer Stempel, Anne Rowan, and Lydia Williams for assistance with animal care.

Funding: this work was supported by an Australian Government Research Training Program Scholarship, a UNSW High Degree for Research Completion Scholarship, and a UNSW Writing Scholarship to L.A.F., as well as by Australian Research Council (DP190102511, DP210102700) and the National Health and Medical Research Council (GNT1165990) grants to J.B.G. and M.M.

DECLARATION OF INTERESTS

The authors declare no competing interests.

Received: July 31, 2023

Revised: October 11, 2023

Accepted: February 15, 2024

Published: February 20, 2024

REFERENCES

- Graybiel, A.M. (1998). The Basal Ganglia and Chunking of Action Repertoires. *Neurobiol. Learn. Mem.* 70, 119–136. <https://doi.org/10.1006/nlme.1998.3843>.
- Lashley, K.S. (1951). *The problem of serial order in behavior. In Cerebral mechanisms in behavior; the Hixon Symposium (Wiley), pp. 112–146.*
- Rosenbaum, D.A., Kenny, S.B., and Derr, M.A. (1983). Hierarchical control of rapid movement sequences. *J. Exp. Psychol. Hum. Percept. Perform.* 9, 86–102. <https://doi.org/10.1037/0096-1523.9.1.86>.
- Saling, L.L., and Phillips, J.G. (2007). Automatic behaviour: Efficient not mindless. *Brain Res. Bull.* 73, 1–20. <https://doi.org/10.1016/j.brainresbull.2007.02.009>.
- Sternberg, S., Monsell, S., Knoll, R.L., and Wright, C.E. (1978). 6 - The Latency and Duration of Rapid Movement Sequences: Comparisons of Speech and Typewriting. In *Information Processing in Motor Control and Learning*, G.E. Stelmach, ed. (Academic Press), pp. 117–152. <https://doi.org/10.1016/B978-0-12-665960-3.50011-6>.
- Terrace, H.S. (1987). Chunking by a pigeon in a serial learning task. *Nature* 325, 149–151. <https://doi.org/10.1038/325149a0>.
- Sternad, D. (2018). It's not (only) the mean that matters: variability, noise and exploration in skill learning. *Curr. Opin. Behav. Sci.* 20, 183–195. <https://doi.org/10.1016/j.cobeha.2018.01.004>.
- Dezfouli, A., Balleine, B.W., and Nock, R. (2019). Optimal response vigor and choice under non-stationary outcome values. *Psychon. Bull. Rev.* 26, 182–204. <https://doi.org/10.3758/s13423-018-1500-3>.
- McSweeney, F.K., and Roll, J.M. (1993). Responding Changes Systematically Within Sessions During Conditioning Procedures. *J. Exp. Anal. Behav.* 60, 621–640. <https://doi.org/10.1901/jeab.1993.60-621>.
- Neuringer, A. (2002). Operant variability: Evidence, functions, and theory. *Psychon. Bull. Rev.* 9, 672–705. <https://doi.org/10.3758/BF03196324>.
- Light, K.R., Cotten, B., Malekan, T., Dewil, S., Bailey, M.R., Gallistel, C.R., and Balsam, P.D. (2019). Evidence for a Mixed Timing and Counting Strategy in Mice Performing a Mechner Counting Task. *Front. Behav. Neurosci.* 13, 109. <https://doi.org/10.3389/fnbeh.2019.00109>.
- Balleine, B.W. (2019). The Meaning of Behavior: Discriminating Reflex and Volition in the Brain. *Neuron* 104, 47–62. <https://doi.org/10.1016/j.neuron.2019.09.024>.
- Balleine, B.W., Delgado, M.R., and Hikosaka, O. (2007). The Role of the Dorsal Striatum in Reward and Decision-Making. *J. Neurosci.* 27, 8161–8165. <https://doi.org/10.1523/JNEUROSCI.1554-07.2007>.
- Balleine, B.W., and O'Doherty, J.P. (2010). Human and Rodent Homologies in Action Control: Corticostriatal Determinants of Goal-Directed and Habitual Action. *Neuropsychopharmacology* 35, 48–69. <https://doi.org/10.1038/npp.2009.131>.
- Ostlund, S.B., and Balleine, B.W. (2005). Lesions of Medial Prefrontal Cortex Disrupt the Acquisition But Not the Expression of Goal-Directed Learning. *J. Neurosci.* 25, 7763–7770. <https://doi.org/10.1523/JNEUROSCI.1921-05.2005>.
- Yin, H.H., Knowlton, B.J., and Balleine, B.W. (2004). Lesions of dorsolateral striatum preserve outcome expectancy but disrupt habit formation in instrumental learning. *Eur. J. Neurosci.* 19, 181–189. <https://doi.org/10.1111/j.1460-9568.2004.03095.x>.
- Yin, H.H., Knowlton, B.J., and Balleine, B.W. (2006). Inactivation of dorsolateral striatum enhances sensitivity to changes in the action–outcome contingency in instrumental conditioning. *Behav. Brain Res.* 166, 189–196. <https://doi.org/10.1016/j.bbr.2005.07.012>.
- Kupferschmidt, D.A., Juczewski, K., Cui, G., Johnson, K.A., and Lovinger, D.M. (2017). Parallel, but Dissociable, Processing in Discrete Corticostriatal Inputs Encodes Skill Learning. *Neuron* 96, 476–489.e5. <https://doi.org/10.1016/j.neuron.2017.09.040>.
- Kita, T., and Kita, H. (2012). The Subthalamic Nucleus Is One of Multiple Innervation Sites for Long-Range Corticofugal Axons: A Single-Axon Tracing Study in the Rat. *J. Neurosci.* 32, 5990–5999. <https://doi.org/10.1523/JNEUROSCI.5717-11.2012>.
- Pimentel-Farfan, A.K., Báez-Cordero, A.S., Peña-Rangel, T.M., and Rueda-Orozco, P.E. (2022). Cortico-striatal circuits for bilaterally coordinated movements. *Sci. Adv.* 8, eabk2241. <https://doi.org/10.1126/sciadv.abk2241>.
- Nelson, A., Abdelmesih, B., and Costa, R.M. (2021). Corticospinal populations broadcast complex motor signals to coordinated spinal and striatal circuits. *Nat. Neurosci.* 24, 1721–1732. <https://doi.org/10.1038/s41593-021-00939-w>.
- Karube, F., Takahashi, S., Kobayashi, K., and Fujiyama, F. (2019). Motor cortex can directly drive the globus pallidus neurons in a projection neuron type-dependent manner in the rat. *Elife* 8, e49511. <https://doi.org/10.7554/eLife.49511>.
- Park, J., Phillips, J.W., Guo, J.-Z., Martin, K.A., Hantman, A.W., and Dudman, J.T. (2022). Motor cortical output for skilled forelimb movement is selectively distributed across projection neuron classes. *Sci. Adv.* 8, eabj5167. <https://doi.org/10.1126/sciadv.abj5167>.
- Jin, D.Z., Fujii, N., and Graybiel, A.M. (2009). Neural representation of time in cortico-basal ganglia circuits. *Proc. Natl. Acad. Sci. USA* 106, 19156–19161. <https://doi.org/10.1073/pnas.0909881106>.
- Jin, X., Tecuapetla, F., and Costa, R.M. (2014). Basal ganglia subcircuits distinctively encode the parsing and concatenation of action sequences. *Nat. Neurosci.* 17, 423–430.
- Jin, X., and Costa, R.M. (2010). Start/stop signals emerge in nigrostriatal circuits during sequence learning. *Nature* 466, 457–462. <https://doi.org/10.1038/nature09263>.
- Matamalas, M., Skrbis, Z., Bailey, M.R., Balsam, P.D., Balleine, B.W., Götz, J., and Bertran-Gonzalez, J. (2017). A corticostriatal deficit promotes temporal distortion of automatic action in ageing. *Elife* 6, e29908. <https://doi.org/10.7554/eLife.29908>.
- Mello, G.B.M., Soares, S., and Paton, J.J. (2015). A Scalable Population Code for Time in the Striatum. *Curr. Biol.* 25, 1113–1122. <https://doi.org/10.1016/j.cub.2015.02.036>.
- Tecuapetla, F., Jin, X., Lima, S.Q., and Costa, R.M. (2016). Complementary Contributions of Striatal Projection Pathways to Action Initiation and Execution. *Cell* 166, 703–715. <https://doi.org/10.1016/j.cell.2016.06.032>.
- Garr, E., and Delamater, A.R. (2020). Chemogenetic inhibition in the dorsal striatum reveals regional specificity of direct and indirect pathway control of action sequencing. *Neurobiol. Learn. Mem.* 169, 107169. <https://doi.org/10.1016/j.nlm.2020.107169>.
- Rueda-Orozco, P.E., and Robbe, D. (2015). The striatum multiplexes contextual and kinematic information to constrain motor habits execution. *Nat. Neurosci.* 18, 453–460. <https://doi.org/10.1038/nn.3924>.
- Mechner, F. (1958). Probability Relations Within Response Sequences Under Ratio Reinforcement. *J. Exp. Anal. Behav.* 1,

- 109–121. <https://doi.org/10.1901/jeab.1958.1-109>.
33. Dhawale, A.K., Wolff, S.B.E., Ko, R., and Ólveczky, B.P. (2021). The basal ganglia control the detailed kinematics of learned motor skills. *Nat. Neurosci.* 24, 1256–1269. <https://doi.org/10.1038/s41593-021-00889-3>.
 34. Jurado-Parras, M.-T., Safaie, M., Sarno, S., Louis, J., Karoutchi, C., Berret, B., and Robbe, D. (2020). The Dorsal Striatum Energizes Motor Routines. *Curr. Biol.* 30, 4362–4372.e6. <https://doi.org/10.1016/j.cub.2020.08.049>.
 35. Yin, H.H. (2010). The Sensorimotor Striatum Is Necessary for Serial Order Learning. *J. Neurosci.* 30, 14719–14723.
 36. Kawai, R., Markman, T., Poddar, R., Ko, R., Fantana, A.L., Dhawale, A.K., Kampff, A.R., and Ólveczky, B.P. (2015). Motor Cortex Is Required for Learning but Not for Executing a Motor Skill. *Neuron* 86, 800–812. <https://doi.org/10.1016/j.neuron.2015.03.024>.
 37. Gradinaru, V., Zhang, F., Ramakrishnan, C., Mattis, J., Prakash, R., Diester, I., Goshen, I., Thompson, K.R., and Deisseroth, K. (2010). Molecular and Cellular Approaches for Diversifying and Extending Optogenetics. *Cell* 141, 154–165. <https://doi.org/10.1016/j.cell.2010.02.037>.
 38. Yang, C.F., Chiang, M.C., Gray, D.C., Prabhakaran, M., Alvarado, M., Juntti, S.A., Unger, E.K., Wells, J.A., and Shah, N.M. (2013). Sexually Dimorphic Neurons in the Ventromedial Hypothalamus Govern Mating in Both Sexes and Aggression in Males. *Cell* 153, 896–909. <https://doi.org/10.1016/j.cell.2013.04.017>.
 39. Giffurda, R., Li Volsi, G., Maugeri, G., and Perciavalle, V. (1985). Influences of pyramidal tract on the subthalamic nucleus in the cat. *Neurosci. Lett.* 54, 231–235. [https://doi.org/10.1016/S0304-3940\(85\)80084-7](https://doi.org/10.1016/S0304-3940(85)80084-7).
 40. Nambu, A., Tokuno, H., and Takada, M. (2002). Functional significance of the cortico-subthalamic-pallidal ‘hyperdirect’ pathway. *Neurosci. Res.* 43, 111–117. [https://doi.org/10.1016/S0168-0102\(02\)00027-5](https://doi.org/10.1016/S0168-0102(02)00027-5).
 41. Oh, S.W., Harris, J.A., Ng, L., Winslow, B., Cain, N., Mihalas, S., Wang, Q., Lau, C., Kuan, L., Henry, A.M., et al. (2014). A mesoscale connectome of the mouse brain. *Nature* 508, 207–214. <https://doi.org/10.1038/nature13186>.
 42. Winnubst, J., Bas, E., Ferreira, T.A., Wu, Z., Economo, M.N., Edson, P., Arthur, B.J., Bruns, C., Rokicki, K., Schauder, D., et al. (2019). Reconstruction of 1,000 Projection Neurons Reveals New Cell Types and Organization of Long-Range Connectivity in the Mouse Brain. *Cell* 179, 268–281.e13. <https://doi.org/10.1016/j.cell.2019.07.042>.
 43. Fisher, S.D., Ferguson, L.A., Bertran-Gonzalez, J., and Balleine, B.W. (2020). Amygdala-Cortical Control of Striatal Plasticity Drives the Acquisition of Goal-Directed Action. *Curr. Biol.* 30, 4541–4546.e5. <https://doi.org/10.1016/j.cub.2020.08.090>.
 44. Zhang, S., Xu, M., Chang, W.-C., Ma, C., Hoang Do, J.P., Jeong, D., Lei, T., Fan, J.L., and Dan, Y. (2016). Organization of long-range inputs and outputs of frontal cortex for top-down control. *Nat. Neurosci.* 19, 1733–1742. <https://doi.org/10.1038/nn.4417>.
 45. Garr, E., and Delamater, A.R. (2019). Exploring the relationship between actions, habits, and automaticity in an action sequence task. *Learn. Mem.* 26, 128–132. <https://doi.org/10.1101/lm.048645.118>.
 46. Gibbon, J. (1977). Scalar expectancy theory and Weber’s law in animal timing. *Psychol. Rev.* 84, 279–325. <https://doi.org/10.1037/0033-295X.84.3.279>.
 47. Gibbon, J., Church, R.M., and Meck, W.H. (1984). Scalar Timing in Memory. *Ann. N. Y. Acad. Sci.* 423, 52–77. <https://doi.org/10.1111/j.1749-6632.1984.tb23417.x>.
 48. Matell, M.S., Meck, W.H., and Nicolelis, M.A.L. (2003). Interval timing and the encoding of signal duration by ensembles of cortical and striatal neurons. *Behav. Neurosci.* 117, 760–773. <https://doi.org/10.1037/0735-7044.117.4.760>.
 49. Adam, E.M., Johns, T., and Sur, M. (2022). Dynamic control of visually guided locomotion through corticosubthalamic projections. *Cell Rep.* 40, 111139. <https://doi.org/10.1016/j.celrep.2022.111139>.
 50. Koketsu, D., Chiken, S., Hisatsune, T., Miyachi, S., and Nambu, A. (2021). Elimination of the cortico-subthalamic hyperdirect pathway induces motor hyperactivity in mice. *J. Neurosci.* 41, 5502–5510. <https://doi.org/10.1523/JNEUROSCI.1330-20.2021>.
 51. Baunez, C., Christakou, A., Chudasama, Y., Forni, C., and Robbins, T.W. (2007). Bilateral high-frequency stimulation of the subthalamic nucleus on attentional performance: transient deleterious effects and enhanced motivation in both intact and parkinsonian rats. *Eur. J. Neurosci.* 25, 1187–1194. <https://doi.org/10.1111/j.1460-9568.2007.05373.x>.
 52. Baunez, C., and Robbins, T.W. (1997). Bilateral Lesions of the Subthalamic Nucleus Induce Multiple Deficits in an Attentional Task in Rats. *Eur. J. Neurosci.* 9, 2086–2099. <https://doi.org/10.1111/j.1460-9568.1997.tb01376.x>.
 53. Frank, M.J. (2006). Hold your horses: A dynamic computational role for the subthalamic nucleus in decision making. *Neural Netw.* 19, 1120–1136. <https://doi.org/10.1016/j.neunet.2006.03.006>.
 54. Frank, M.J., Samanta, J., Moustafa, A.A., and Sherman, S.J. (2007). Hold your horses: impulsivity, deep brain stimulation, and medication in parkinsonism. *Science* 318, 1309–1312.
 55. Bradfield, L.A., Bertran-Gonzalez, J., Chieng, B., and Balleine, B.W. (2013). The Thalamostriatal Pathway and Cholinergic Control of Goal-Directed Action: Interlacing New with Existing Learning in the Striatum. *Neuron* 79, 153–166. <https://doi.org/10.1016/j.neuron.2013.04.039>.
 56. Bradfield, L.A., Matamalas, M., and Bertran-Gonzalez, J. (2018). The Thalamostriatal Pathway and the Hierarchical Control of Action. *Neuron* 100, 521–523. <https://doi.org/10.1016/j.neuron.2018.10.041>.
 57. Matamalas, M., McGovern, A.E., Mi, J.D., Mazzone, S.B., Balleine, B.W., and Bertran-Gonzalez, J. (2020). Local D2- to D1-neuron transmodulation updates goal-directed learning in the striatum. *Science* 367, 549–555. <https://doi.org/10.1126/science.aaz5751>.
 58. Aristieta, A., Barresi, M., Azizpour Lindi, S., Barrière, G., Courtand, G., de la Crompe, B., Guilhemsang, L., Gauthier, S., Fioramonti, S., Baufretton, J., and Mallet, N.P. (2021). A Disynaptic Circuit in the Globus Pallidus Controls Locomotion Inhibition. *Curr. Biol.* 31, 707–721.e7. <https://doi.org/10.1016/j.cub.2020.11.019>.
 59. Logan, G.D., and Cowan, W.B. (1984). On the ability to inhibit thought and action: A theory of an act of control. *Psychol. Rev.* 91, 295–327. <https://doi.org/10.1037/0033-295X.91.3.295>.
 60. Mallet, N., Schmidt, R., Leventhal, D., Chen, F., Amer, N., Boraud, T., and Berke, J.D. (2016). Arkyppallidal Cells Send a Stop Signal to Striatum. *Neuron* 89, 308–316. <https://doi.org/10.1016/j.neuron.2015.12.017>.
 61. Schmidt, R., and Berke, J.D. (2017). A Pause-then-Cancel model of stopping: evidence from basal ganglia neurophysiology. *Philos. Trans. R. Soc. Lond. B Biol. Sci.* 372, 20160202. <https://doi.org/10.1098/rstb.2016.0202>.
 62. Neuringer, A., Deiss, C., and Olson, G. (2000). Reinforced variability and operant learning. *J. Exp. Psychol. Anim. Behav. Process.* 26, 98–111. <https://doi.org/10.1037/0097-7403.26.1.98>.
 63. Cohen, J. (1977). *Statistical Power Analysis for the Behavioral Sciences*, Revised Edition (Academic Press). <https://doi.org/10.1016/B978-0-12-179060-8.50001-3>.
 64. Paxinos, G., and Franklin, K.B.J. (2007). *The Mouse Brain in Stereotaxic Coordinates*, 3rd edition (Academic Press).
 65. Schindelin, J., Arganda-Carreras, I., Frise, E., Kaynig, V., Longair, M., Pietzsch, T., Preibisch, S., Rueden, C., Saalfeld, S., Schmid, B., et al. (2012). Fiji: an open-source platform for biological-image analysis. *Nat. Methods* 9, 676–682. <https://doi.org/10.1038/nmeth.2019>.

STAR★METHODS

KEY RESOURCES TABLE

REAGENT or RESOURCE	SOURCE	IDENTIFIER
Bacterial and virus strains		
rAAV5/CMV-HI-EGFP-Cre-WPRE	AddGene	Cat #105540; RRID:Addgene_105540
rAAV5/Flex-taCasp3-TEVP	UNC Vector Core	Plasmid #45580; RRID:Addgene_45580
AAV2/5-hSyn-FLEX-mGFP-2A-Synaptophysin-mRuby	AddGene	Plasmid #71760; RRID:Addgene_71760
rAAV2/EF1a-mCherry-IRES-WGA-Cre	UNC Vector Core	Cat 55632-AAVrg; RRID:Addgene_55632
Chemicals, peptides, and recombinant proteins		
Nissl: red fluorescent stain	Thermo Fisher Scientific	Cat# N21482, RRID:AB_2620170
Deposited data		
Raw and analyzed datasets	This paper	https://doi.org/10.6084/m9.figshare.21640763
Experimental models: Organisms/strains		
DRD2-EGFP-F1 hybrid mice (C57Bl/6 x Drd2-eGFP) C57Bl/6J–Quackenbush hybrid transgenic mice carrying bacterial artificial chromosome (BAC) that expresses enhanced green fluorescent protein (BAC-EGFP) under the control of the D2R promoter (Drd2-EGFP)	Bred and maintained in-house, UNSW, AU. (originally sourced from Jackson laboratory, US)	RRID: MMRRC_000230-UNC
C57Bl/6 mice	Animal Resource Center, AU	RRID:IMSR_ARC:B6
Software and algorithms		
Med-PC IV – behavioral data collection	Med-Associates	https://www.med-associates.com
MATLAB 2018–2020 – analysis	MathWorks	https://www.mathworks.com/products/matlab.html
NIS-Elements – confocal capture	Nikon	https://www.microscope.healthcare.nikon.com/products/software/niselements
Fiji/ImageJ 1.52	National Institutes of Health, USA	https://imagej.nih.gov/ij/
SPSS Statistics 26	IBM	https://www.ibm.com/au-en/analytics/spss-statistics-software
Prism	GraphPad	Version 9
Code	This paper	https://doi.org/10.6084/m9.figshare.21640835
Other		
Nanoject III	Drummond Scientific Company	Cat# 3-000-207
20 mg Grain pellets	Bio-Serv Technologies	Cat# F0163

RESOURCE AVAILABILITY

Lead contact

Further information and requests for resources should be directed to and will be fulfilled by the Lead Contact, Jesus Bertran-Gonzalez (j.bertran@unsw.edu.au).

Materials availability

This study did not generate new unique reagents.

Data and code availability

- All original raw data have been deposited at Figshare: <https://doi.org/10.6084/m9.figshare.21640763>.

- All original code has been deposited at Figshare: <https://doi.org/10.6084/m9.figshare.21640835>.
- Any additional information required to reanalyze the data reported in this work paper is available from the [lead contact](#) upon request.

EXPERIMENTAL MODEL AND STUDY PARTICIPANT DETAILS

All experimental procedures were approved by the Animal Care and Ethics Committee at the University of New South Wales (application numbers 17/20B and 19/147A) in accordance with the Australian Code of Practice for the Care and Use of Animals for Scientific Purposes (National Health and Medical Research Council, 2013) and Animal Care and Ethics Committee (ACEC) guidelines. Subjects for all experiments were mice (*Mus musculus*). A total of 35 mice (C57Bl/6 and C57Bl/6 x Drd2-eGFP hybrids) including both male and females ranging from 3 to 6 months old were used in this study. Mouse home cages were stored in a climate-controlled colony room. Light/dark cycles rotated every 12 h and cage air was ventilated with an air handling unit (Tecniplast, Italy). Cages were made of clear plastic and enriched with a blue plastic igloo, a red plastic cylinder and dried corn-based bedding. Mice were grouped into 2–6 littermates per home cage and had *ad libitum* access to water and standardised lab chow up to 2 days prior to the onset of the behavioral tasks.

A total sample size of 16 mice was used in this study to account for up to two exclusions (G*power sample size report: Effect size $f(V) = 1.581139$; α err prob = 0.05; power (1- β err prob) = 0.95; Actual power = 0.9675909; Total sample size = 14).⁶³ Sixteen female and sixteen male DRD2-EGFP-F1 hybrid mice (RRID:MMRRC_000230-UNC, originally sourced from Jackson laboratory, US) were bred and maintained in-house and used in the behavioral observation study. Three male C57BL/6 mice (RRID:IMSR_ARC:B6; Animal Resource Center, AU) were included in the viral tracing study of accessory hyperdirect pathways. Sixteen male C57BL/6 mice were used in the study of motor cortex driven function of post-synaptic cells in the DLS. Mice were randomly assigned into groups without exclusions. Any differences in the female-male sex ratios were due to limitations in availability.

METHOD DETAILS

Behavioral procedures and analysis

Apparatus

All behavioral tasks were performed within operant conditioning chambers (Med Associates Inc, US) that were contained within light and sound attenuating cubicles. Each chamber was fitted with a pellet dispenser capable of delivering 20 mg grain pellets (#F0163, Bio-Serv, US) to a recessed feeding magazine, and two retractable levers separated by the magazine. An infrared photobeam spanned the entrance to the magazine, and any breaks in this photobeam were recorded as magazine entries. A light (3W, 24V) was situated at the top-center of the rear chamber wall, and was illuminated during behavioral experiments. Behavioral tasks were programmed using MedState notation (Pascal programming language) in order to control the extension and retraction of levers, delivery of pellets, and to turn the house light on and off. Programs were executed and behavioral responses (i.e., lever presses or magazine entries) and outcomes (i.e., pellet delivery) were detected and outputted to.txt files using Med-PC software (Med Associates Inc, US).

Food restriction

Animals' access to food was restricted from 2 days prior to and throughout the behavioral training period. Every 24hrs, following behavioral training, approximately 2.3 g of standard lab chow per animal was left in their home cage. Mice weights and health indicators were measured and recorded each day, ensuring animals maintained a body weight above 85% of their free-feeding weight and a healthy disposition.

Magazine training

In all behavioral experiments, animals underwent one magazine training session per day for two days prior to instrumental training. Each mouse was assigned a chamber, which was sustained throughout the experiment. During magazine training, levers were retracted and 20 grain pellets (20 mg, 3.35 kcal/g each) were delivered to the magazine on a random-time 60-s schedule over 20 min.

Tandem lever sequence task

All instrumental training began with the insertion of the lever/s and the illumination of the chamber light and finished with the retraction of the lever/s and the extinction of the light. Each session occurred once a day, lasting up to 45 min or 20 pellet deliveries (whichever came first). In the 'tandem sequence task', instrumental training began with continuous reinforcement (CRF) on a single lever ('End lever') for 4 sessions, during which, each lever press resulted in the delivery of a grain pellet reward. In the following 4 training sessions, a second lever was extended in tandem with the lever that was previously rewarded. Animals were now required to press once on the newly introduced lever ('Sequence lever'), prior to pressing the previously rewarded lever ('End lever') in order to receive a reward. The number of presses required (fixed ratio - FR) on the Sequence lever increased by two presses every four sessions from FR1 to FR3 to FR5 to FR7 in the study that focused on motor cortical driven lesion of the DLS. In the behavioral observation study, however, the required presses on the Sequence lever increased by two presses every four sessions from FR1 to FR3 to FR5, then sustained on FR5 for seven sessions to observe the influence of overtraining on well-established sequences. The left and right position of levers that served as either the Sequence or End lever were counterbalanced within each group.

Behavioral analysis

MedState notation scripts coded individual events as discrete numbers: Sequence lever press (1), End lever press (2), pellet delivery (3), and magazine entry (4). When any of these events occurred during training, the coded number was stored chronologically and timestamped (0.01s time resolution) in an output array and saved to a.txt file. MATLAB scripts extracted the raw data from these.txt files and performed data organisational functions, behavioral quantifications, and data representations. Data organisation comprised alignment of coded action numbers with timestamp data points, such that each action was indexed to its corresponding time of performance in the session. Data was further organised by coding event transition types. Here, all combinations of transitions between any of the four coded events (Sequence lever press, End lever press, pellet delivery, and magazine entry) were given unique numeric identifiers used to find their position in an action sequence. In addition to within-sequence analysis, sequences could be categorised based on their association with reward: sequences immediately followed by reward delivery were called 'Successful'; all sequences that did not result in reward were considered 'Unsuccessful'; and all sequences that occurred — irrespective of reward — were termed 'All' sequences. Other more general measures of behavior could also be extracted from this numerically action-coded dataset, including: totals and rates of Sequence lever and End lever presses, total reward deliveries and rates, and total magazine entries and rates. Analysis of the chronological arrangement of sequence segments required indexing a specific numeric identifier within a sequence and calculating the time between this and the numeric identifier of interest. For example, when investigating the duration of FR3-5 segments in FR5 training, the time from the 3rd press to the 5th press was calculated by subtracting the time at which the 5th press in the sequence occurred during the session from the time the 3rd press occurred in the session; the remainder being the time between these two events. Each of these times were arranged chronologically for each mouse within a session and aligned between mice. This allowed for the collective comparison of segment durations of all mice at any given chronological position to be compared against the segment durations of all mice occurring at different chronological positions.

Viral procedures

Stereotaxic surgical injection of viruses

Animals were anesthetized using isoflurane gas (Laser Animal Health, Pharmachem, AU). Induction commenced with 3% isoflurane delivered in oxygen at 0.5L/min in an induction chamber. After approximately 5 min animals were transferred to a stereotaxic frame (Kopf instruments) and fitted to the face mask and ear bars, and maintained on 1–1.5% isoflurane mixture with oxygen (0.5L/min). Fur above the cranium was removed with scissors and hair removal cream and the area was sanitised with betadine antiseptic solution. Bupivacaine (0.1 mL), a local anesthetic, was subcutaneously administered at the surgical site, while Carprofen analgesic (0.4 mL/kg) and saline (1 mL) were delivered subcutaneously at the lower back. An incision was made on the scalp to reveal the skull, and animal head placement was adjusted to align bregma and lambda skull landmarks on the sagittal and transverse planes. Injection sites were determined by anterior-posterior, medial-lateral, and dorsoventral (from skull) axis coordinates from "The Mouse Brain in stereotaxic coordinates, 3rd edition",⁶⁴ and from pilot injection studies. Using a 26-gauge needle mounted to the stereotaxic holder, holes (~0.2mm width) through the skull were carefully pierced above injection sites relative to bregma. Infusion fluid (virus or control solution) was loaded into a microinjector (Nanoject III; Drummond Scientific Company), and its pulled glass capillary pipette tip (GC100TF-15; Harvard Apparatus) pulled using a micropipette puller (P-97, Sutter Instrument) and lowered through the puncture hole to the injection site. A 2-min waiting period occurred prior to the injection, which was infused at a rate of 2 nL/s; total injection volumes varied depending on experiment (see below for details). Following the injection, infusion fluid was left to rest for 3 min before retracting the microinjector pipette tip. The incision site on the scalp was sutured with surgical thread and treated with Betadine Antiseptic Topical Ointment and sealed with tissue adhesive (3M Vetbond). The delivery of anesthetic was stopped, and animals were laid on a heat mat for 5 min prior to placing them in a recovery cage.

Circuit-specific ablation of striatal neurons receiving motor cortical projections

To selectively ablate the post-synaptic targets of the motor cortical projections in the DLS, a combination of interacting viral systems was used. We stereotaxically injected a first AAV (500 nL) with anterograde transsynaptic profile expressing Cre (AAV2-EF1a-mCherry-IRES-WGA-Cre; Addgene #55632, RRID:Addgene_55632)^{37,38,43} into the M1 region of the cortex (AP: -2.06 mm; ML: +1.58; DV: -4.9 [from skull]). The second viral injection was targeted to the DLS region of the dorsal striatum (coordinate: AP: 0 mm; ML: +2.65; DV: -3.0 [from skull]); volume (500–650 nL). Half of the animals received the AAV-Flex-taCasp3-TEVp virus (Addgene #45580, RRID:Addgene_45580), which induces expression of a designer procaspase 3 (taCasp3) that is lacking endogenous caspase cleavage sites but is sensitive to the heterologous tobacco etch virus protease (TEVp) in the presence of Cre (Group Lesion). The other half received, in the same region, an AAV5-EF1A-DIO-eYFP control virus expressing Cre-dependent eYFP (group Sham).

Viral tracing of accessory collaterals in motor corticofugal pathways

To assess if cortical descending pathways originated in primary motor cortex (M1) and collateralising to the subthalamic nucleus (STN) also send accessory projections from the same motor cortical neurons to the posterior dorsal striatum (pDStr) and/or to the external segment of the globus pallidus (GPe), a combination of two virus was injected intracranially into the STN and M1. First, 85 nL of retro-cre-EGFP (rAAV5-CMV-HI-EGFP-Cre-WPRE; Addgene #105545, RRID:Addgene_105545) was infused unilaterally into the STN (AP: -2.06 mm; ML: +1.58; DV: -4.9). Then, 400 nL of antero-mGFP-Syp-mRuby (AAV2-5-hSyn-FLEX-mGFP-2A-Synaptophysin-mRuby; Addgene #71760, RRID:Addgene_71760) was infused unilaterally into the M1 (AP: -1.78 mm; ML: +1.75; DV: -1.23) ipsilateral to the STN injection. This method

allows for visualisation of both axonal projections (mGFP) and pre-synaptic boutons (Syp-mRuby) in anterograde synaptic territories, such as the pDStr, GPe and STN of Cre expressing motor cortical cells that are known to project to the STN.

Tissue processing and immunofluorescence labeling

Transcardial fixation and tissue sectioning

In behavioral experiments, animals were anesthetised with isoflurane gas (4% in air; Laser Animal Health, Pharmachem, AU) for 1 min inside a sealed container. A lethal intraperitoneal injection of sodium pentobarbital (0.5–0.9 mL, 500 mg/kg; Virbac Pty. Ltd., Australia) was administered, and follow-up paw and tail reflex checks occurred before commencing the perfusion. Mice were perfused transcardially for 10 min using an air pressure system (15 mL/min flow) with 4% paraformaldehyde (PFA) in a solution of 0.1 M sodium phosphate buffer (pH 7.4). Brains were extracted and stored individually in PFA solution at 4°C for 12–48 hrs before sectioning. Consecutive 30 μ m coronal sections of brain were sliced in 0.1 M phosphate buffer solution (PBS) using a vibratome (LEICA VT1000S, Leica Microsystems, Germany). Sections were sliced in an anterior-posterior direction, spanning regions of interest including: motor cortex, striatum, external globus pallidus and subthalamic nucleus. Free-floating sections were stored in a cryoprotectant solution (0.1 M sodium phosphate buffer, 30% v/v ethylene glycol, 30% v/v glycerol, 0.25 M Tris buffer) at –20°C until immunofluorescence procedures.

Immunofluorescence labeling

Free-floating sections were rinsed three times in Tris-buffered saline (TBS) solution (0.25 M Tris and 0.5 M NaCl at pH 7.4) for 10 min in an orbital shaker at room temperature. In the viral tracing experiment, sections were mounted on Superfrost Plus coated slides (Thermo Fisher Scientific) and Vectashield fluorescence medium (Vector Laboratories) was applied before placing a coverslip on top. The study that focused on identifying a motor cortical driven lesion of the DLS required Nissl staining (640/660 deep-red fluorescent Nissl Stain, cat. No. 21483; 1:500; Thermo Fisher Scientific, US) for cell quantification. Sections were washed three times for 10 min in TBS at room temperature before permeabilisation in 0.5% Triton X-100 in TBS for 2 hrs, followed by three 10-min washes in TBS at room temperature. Sections were then incubated for 1 h at room temperature in Nissl stain, followed by three 10-min washes in TBS at room temperature before mounting. Slides were stored at 4°C and images were captured within 72 hrs of mounting.

Image acquisition and quantitative analysis

Spinning disk confocal microscopy

A wide-field spinning disk confocal system was used to capture images of mouse brain sections. A Discovery multi-modal imaging platform and Zyla 4.2 sCMOS camera (Andor Technology) was added to a Nikon Eclipse TiE microscope body with a motorized stage and the Nikon Perfect Focus System, with image acquisition controlled by Nikon NIS-Elements software used to capture and produce mosaic images with 20 \times optical magnification, 16-bit pixel depth at 3.0269 pixels/ μ m image resolution. Up to three channels (488 nm, 561 nm and 640 nm lasers) were captured. An Olympus Confocal microscope (Olympus BX61WI) was also used to capture images at cortical injection sites, at 40 \times optical magnification at 3.2258 pixels/ μ m resolution and up to 2 channels (473 nm and 559 nm lasers) per image.

Nuclear and synaptic varicosity/bouton mapping

Spinning disk confocal images from each animal were processed using ImageJ/Fiji software (v. 1.53c).⁶⁵ Freehand selections were used to create regional outlines of the DStr, GPe and STN and the regional area (mm²) and Cartesian (x,y) outline coordinates were measured. Binary images were generated from thresholds based on pixel intensity of biofluorescence in the soma (nissl fluorescence) or the synaptic boutons (Syp-mRuby). These binary images were used to quantify fluorescence with the *Analyze Particle* command, which locates the edge of an object based on its roundness and size, and determines the particles' cartesian (x,y) coordinates of its centroid position. Data on the position of the fluorescent particles and the regional outline were imported into MATLAB (MathWorks). The *inpolygon* function returned a list of points within the regional outline, and a distribution of the particles was reconstructed for each slice with a line-plot of the regional outline and scatterplot of cartesian centroid points. In the viral tracing study, the *densityplot* function was used to generate a colourmap relative to the spatial density of particles. Particle density was then calculated as the total number of particles within the regional outline area (particles/mm²).

Allen Mouse Brain Connectivity Atlas resource methodology

The Adult Mouse Connectivity Atlas is a large-scale searchable image database containing serial two-photon tomographic images of axonal projections labeled by viral (rAAV) tracers. The Atlas is built on an extensive library of experiments using enhanced green fluorescent protein (EGFP)-expressing adeno-associated viral vectors that are used to trace axonal projections from defined regions and cell types. These are imaged through high-throughput serial two-photon tomography to capture the EGFP-labelled axons throughout the brain. A computational model yields insights into connective strength, distribution, symmetry and other network properties.⁴¹

Selection of Allen Mouse Brain Connectivity Atlas studies

There are many approaches to searching the Adult Mouse Connectivity Atlas database, outlined here: <http://help.brain-map.org/display/mouseconnectivity/Projection#Projection-Searching>. In order to test the connectivity between the motor cortical regions and STN, we

applied a specific filtered search to both the viral tracer injection site ('Source') and projection target structure ('Target'). Here we inputted both Primary (MOp) and Secondary (MOs) motor cortex as 'Source' structures and the STN as the 'Target' structure. Using the 'Source' and 'Target' search in this way we created a "virtual" anterograde study of the M2/M1 injection site and its projections to the STN. Searching was then filtered by projection density; calculated as a ratio of pixels with signal over all pixels in the structure. Three experiments with the highest projection density to the STN from cortical regions were selected for analysis. The details of these experiments can be found in [Table S2](#).

MouseLight Neuron Browser resource methodology

MouseLight Neuron Browser database includes a growing library of reconstructed cortical neurons in the mouse whose structural paths are registered to the Allen Reference Atlas, so that brain regions containing the neuron's axonal paths and endpoints can be reliably identified.⁴²

Search parameters in MouseLight database

We sought to verify whether motor cortical neurons could emit axon collaterals to multiple basal ganglia stations, namely the dorsal striatum, the GPe and the STN. We also sought to verify whether such neurons existed if thalamic regions around the STN were included instead. Details of each search along with the obtained results are indicated in [Table S3](#).

3D reconstruction of the identified neuron

Neuron AA0245 (<https://doi.org/10.25378/janelia.5527657>) was exported from the Janelia MouseLight browser in JSON format, which contained the complete neuron path, and the Allen region ID for each node on the path. Using a Python (v3.10) script, the path nodes were assigned colors according to their corresponding Allen region IDs. For the whole brain, planned targets, and unplanned targets in turn, the relevant regions of interest (as obtained using the Allen SDK) along with neuron AA0245 (also colored with the relevant assigned region colors) were plotted using Napari, and a resulting snapshot exported with the camera viewport as shown in [Figures 4I–4K](#) and [S5D](#).

QUANTIFICATION AND STATISTICAL ANALYSIS

Statistical analysis was performed predominantly using IBM SPSS Statistics software (version 28; IBM Corporation, NY). The *a priori* alpha level was set at $p < 0.05$. To test the assumption of equal variances between independent groups, Levene's test for equal variances was applied with the null hypothesis that the error variance was equal across groups. If the null hypothesis was rejected, Welch-Satterthwaite corrections to the degrees of freedom were applied (SPSS's 'equality of variance not assumed' option) to any independent samples t-tests (two-tailed). For univariate and repeated measures ANOVA, the homogeneity of variance was tested using Mauchly's test of sphericity. If the assumptions of sphericity were violated, Greenhouse-Geisser corrections were applied. Repeated measures ANOVA calculations require complete data; thus, in instances where a value was missing from a dataset relative to another subject (e.g., when one mouse reached the maximum of 20 rewarded sequences in a session, while another did not), the fitting of a mixed effects model was used to analyze repeated measures data with missing values. A compound symmetry covariance matrix was used in the mixed effects model, and to control for assumptions of homogeneity of variance, Greenhouse-Geisser corrections were applied using Graphpad Prism (version 9; GraphPad Software, US). Linear regression analysis was also applied to infer the relationship between dependent variable/s and their occurrence chronologically. All statistical analyses conducted in this study are included in the [Table S1](#) of the [supplemental information](#). The following information is provided in the table: (1) relevant figure panel, (2) a description of the analysis conducted, (3) the test applied, (4) the dependent variable(s), (5) the independent variable(s), (6) the descriptive statistics results and (7) the p value(s) of each result.